IOP Conf. Series: Journal of Physics: Conf. Series **1037** (2018) 032019 doi:10.1088/1742-6596/1037/3/032019

Sparse-Sensor Placement for Wind Farm Control

J. Annoni[1], T. Taylor[2], C. Bay[1,2,3], K. Johnson[1,2], L. Pao[3], P. Fleming[1], K. Dykes[1]

[1]National Renewable Energy Laboratory, Golden, CO, USA
[2]Colorado School of Mines, Golden, CO, USA
[3]University of Colorado, Boulder, CO, USA

E-mail: jennifer.annoni@nrel.gov

Abstract.

The objective of this paper is to incorporate sparse sensor data to improve flow-field estimates in a wind farm, which can then be used to perform better online wind farm optimization and control. A sparse-sensing algorithm is used to determine the optimal locations of sensors to improve the overall estimation precision of the flow field within the wind farm. This algorithm takes advantage of the dominant atmospheric structures in a wind farm to reconstruct the flow field from point measurements in the field. These measurements, in their optimal locations, have the ability to improve the observability of a wind farm and thus provide faster, more accurate, state estimation.

1. Introduction

Many studies have been done showing that operating all turbines at their own locally optimal operating point leads to suboptimal global performance [1]. Implementing a coordinated wind farm control strategy has the potential to improve the performance of a wind farm [2, 3, 4]. Operating a wind farm with coordinated control of turbines will rely on accurate and timely measurements. Traditionally, sensors are statically placed in locations that are convenient for installation and maintenance rather than targeting locations for optimal measurements, which may change as the wind direction changes. These sensors can be very expensive to install and maintain, limiting the number to be installed, and oftentimes cannot be moved once they are placed/built. In addition, sensors on the back of turbines are often noisy and unreliable. To improve the observability of the wind farm, additional sensors, such as met towers, lidars, etc., should be added in optimal locations to improve controller performance and state estimation [5, 6].

This paper focuses on a sparse data-driven sensor placement algorithm to determine the optimal locations of sensors in a wind farm to improve the observability of a wind farm and thus provide better state estimation and improve the performance of a controller deployed in a wind farm. This approach is based on the work done in [7, 8], where a data-driven approach was used to reconstruct a variety of high-dimensional systems including images and flow fields. This paper applies this algorithm to the wind farm problem and integrates the measurements into a dynamic reduced-order model of a wind farm. Section 2 details the sparse-sensor placement algorithm that leverages data-driven strategies including proper orthogonal decomposition and dynamic mode decomposition [9, 10, 11, 12]. This algorithm is implemented and compares a reduced-order model (described in Section 3.1) with a high-fidelity computational fluid dynamics (CFD)

Content from this work may be used under the terms of the Creative Commons Attribution 3.0 licence. Any further distribution of this work must maintain attribution to the author(s) and the title of the work, journal citation and DOI.
Published under licence by IOP Publishing Ltd

model (described in Section 3.2). The reduced-order model has been combined with the optimal sensor measurements using a Kalman filter. The results are shown in Section 4. Section 5 summarizes the findings and proposes future work.

2. Sparse-Sensor Placement

This section focuses on the algorithm used to determine the sparse-sensor locations in a wind farm. This algorithm is data-driven and takes advantage of the dominant structures and the low-dimensional patterns in a wind farm.

2.1. Proper Orthogonal Decomposition

Proper orthogonal decomposition (POD) provides a low-order approximation of the flow that is capable of capturing dominant structures in the flow. Specifically, POD can be used to extract dominant spatial features from both simulation and experimental data that can be used to uncover structures in the flow [13, 14]. In the wind farm example, this can be done by projecting the wind velocity field onto a set of orthogonal basis functions. POD modes have been used in many previous studies to analyze wind farms [15, 16, 17, 18].

Consider a system modeled by the continuous-time nonlinear dynamics

$$\dot{x}(t) = f(x(t)), \tag{1}$$

where $x \in \mathcal{R}^{n_x}$ is the state vector. The POD modes of this system can be computed from the snapshots of the nonlinear system. A data matrix of the snapshots is formed by

$$X_0 = [x(t_0), \quad x(t_1), \quad ..., \quad x(t_{n_s})] \tag{2}$$

where n_s is the number of snapshots. The POD modes are then computed by taking the singular-value decomposition of the data matrix

$$X_0 = U\Sigma V^T. \tag{3}$$

The POD modes are contained in the columns of U, the relative energy of each mode is contained in the singular values in Σ, and the associated dynamics are in V. The modes provide the spatial component of the flow and are ordered such that the first POD mode is the spatial mode that contains the most energy, representing the dominant structure in the flow.

2.2. Optimal Sparse-Sensor Locations

After the dominant structures have been identified using POD, they will be used to identify sensor locations in a wind farm that minimize the flow-field estimation error [7]. This approach exploits the interactions between turbines to identify sparse measurements in a wind farm.

The objective of this paper is to minimize the error between the actual and estimated state by optimally placing sensors within the flow. It is assumed that the measurements are perfect, i.e., there are no sensor models. Cost of the sensor system is not considered but will be a topic of future research. In addition, this work considers the full flow field; however, future work will also weight portions of the flow that impact wind farm controls the most such as favoring the estimate of far wake dynamics over the near wake dynamics.

In the wind farm control/estimation problem, the state is considered to be the wind velocity throughout the wind farm. The objective function is then

$$\min_{\gamma \in \mathcal{R}^r} \quad \|x - \hat{x}(\gamma)\|_2, \tag{4}$$

where $\gamma = [\gamma_1, \gamma_2, ..., \gamma_r]$ is the index of the sensor location corresponding to the state, r indicates the number of sensors and the order of the model used to determine $\hat{x}$, $\hat{x}$ is the estimated state, and x is the actual state. The estimated state, $\hat{x}$, is computed using a reduced-order model described in Section 3.1, and the actual state, x, is computed from a high-fidelity CFD model described in Section 3.2.

The measurements, y, calculated via

$$y = Cx, \tag{5}$$

where $C = [e_{\gamma_1}, \quad e_{\gamma_2}, \quad ..., \quad e_{\gamma_r}]^T$ and $e_{\gamma_i} \in \mathcal{R}^{n_x}$ is a unit vector at the index γ_i for the location of each sensor. The measurements are then used to estimate the state of the system, $\hat{x}$, and can be incorporated into the system by using filtering approaches (described in Section 3.3).

To solve this optimization problem, POD modes are used to construct the subspace that contains the dominant modes of the system such that the full state, x, can be approximated by

$$\hat{x} = U_r z, \tag{6}$$

where z is the reduced-order state of x projected onto the subspace U_r, where r indicates the number of modes and is equal to the number of sensors. Extensions of this approach show that it is possible to have more measurements than states. However, for this work, we are assuming that the number of reduced-order states is equal to the number of sensors. The measurement equation can be written such that:

$$y = Cx \approx (CU_r)z := Hz. \tag{7}$$

Using these point measurements in the flow, the reduced-order state can be computed as

$$z = (CU_r)^{-1} y \tag{8}$$

and an estimate of the full state can be computed using (6). The optimal sensor locations target the best reconstruction of $\hat{x}$ given the subspace, U_r. To solve this problem, H is optimally conditioned such that $\hat{x}$ is not sensitive to inversion errors in H [8]. Specifically, the spectral content of H is optimized using the trace of H:

$$\gamma_* = \arg\min_{\gamma} \|H^{-1}\|_2, \tag{9}$$

where γ_* are the indices of the optimal sensor locations. Direct optimization (9) is intractable for large systems as this becomes a combinatorial search. Instead, the optimization problem is solved using an approximate greedy solution using a QR factorization with column pivoting [8]. In particular, a QR decomposition is performed on the subspace U_r^T using column pivoting. A column permutation matrix, P, is computed such that

$$U_r^T P^T = QR \tag{10}$$

$$\tag{11}$$

where Q is a unitary matrix, R is an upper-triangular matrix, and P is chosen so that the diagonal elements of R are nonincreasing and is often used for matrices that are rank deficient. This permutation matrix, P, then becomes the measurement matrix $C = P$, where C has entries $[e_{\gamma_1}, \quad e_{\gamma_2}, \quad ..., \quad e_{\gamma_r}]^T$ as stated earlier, which indicates the locations of the point measurements. The QR factorization with column pivoting provides r point measurements that best sample the modes in U_r^T.

3. Modeling

To demonstrate the algorithm presented in the previous section, a reduced-order model is used to estimate the states and a high-fidelity CFD code to simulate the actual states. The measurements of the actual state are integrated into the reduced-order model through a Kalman filter.

3.1. Reduced-Order Model

Dynamic mode decomposition (DMD) is used to construct a reduced-order model that extracts the dominant spatial and temporal information about the flow using POD modes [9, 10, 19]. This method attempts to fit a discrete-time linear system to a set of snapshots from simulation or experiments. Consider a system modeled by the following discrete-time nonlinear dynamics:

$$x_{k+1} = g(x_k), \tag{12}$$

where $x \in \mathcal{R}^{n_x}$ is the state vector, now given in discrete time format as sampled from (1). A collection of snapshot measurements $\{x_k\}_{k=0}^{n_s} \in \mathcal{R}^{n_x}$ is obtained for the system either by simulation or experiments and n_s is the number of snapshots. Assume there is a matrix A that relates the snapshots in time by:

$$x_{k+1} = Ax_k. \tag{13}$$

For the wind farm example, it is assumed that the turbines are operating normally within Region 2 as defined in [20, 21]. The snapshots of the system are defined as

$$\begin{aligned} X_0 &= [x_0, \quad x_1, \quad ..., \quad x_{n_s-1}] \in \mathcal{R}^{n_x \times (n_s-1)} \\ X_1 &= [x_1, \quad x_2, \quad ..., \quad x_{n_s} \quad] \in \mathcal{R}^{n_x \times (n_s-1)}, \end{aligned}$$

where x_k are the snapshots of the full state and n_s is the number of snapshots. The full-order A matrix can be computed via:

$$A = X_1 X_0^{\dagger}, \tag{14}$$

where † indicates the pseudoinverse. This is intractable for high-dimensional systems where n_x is large ($\geq 10^5$). The objective of DMD is to approximate the dynamics of the system by projecting the snapshots onto a low-dimensional subspace. A low-dimensional matrix, F, can be approximated using an orthogonal projection, such as POD. The optimal reduced-order state matrix, F, for this choice is

$$F := U_r^T A U_r = U_r^T X_1 (U_r^T X_0)^{\dagger} = U_r^T X_1 V_r \Sigma_r^{-1}, \tag{15}$$

where r is the dimension of the reduced-order model (and number of sensors) and the corresponding low-rank approximation for the full-order state matrix is

$$A \approx U_r F U_r^T = U_r U_r^T X_1 X_0^{\dagger}. \tag{16}$$

Computing the error, $\|X_1 - AX_0\|_F^2$, directly is computationally intractable for high-dimensional systems. Using the properties of the Frobenius norm, the error of the system can be computed as:

$$\frac{\|X_1 - AX_0\|_F^2}{\|X_1\|_F^2} = \frac{\|Q^T X_1 - F Q^T X_0\|_F^2 + \left(\|X_1\|_F^2 - \|Q^T X_1\|_F^2\right)}{\|X_1\|_F^2} \leq \epsilon, \tag{17}$$

where ϵ is a user-specified error threshold that defines the order of the model. As mentioned previously, the order of the model determines the number of sensors. A higher-order model to estimate $\hat{x}$ translates to a smaller error when comparing the estimated state with the actual state.

The reduced-order model can be written as:

$$z_k = Fz_{k-1} \tag{18}$$

$$y_k = Hz_k, \tag{19}$$

where $\hat{x}$ can be approximated by (6) and compared with the actual state generated by the high-fidelity model described in the next section. DMD has been connected to the Koopman operator that can be used to describe nonlinear systems [22, 23]. Future work will generate a reduced-order model for a wind farm using Koopman modes.

3.2. High-Fidelity Model: Simulator fOr Wind Farm Applications

The Simulator fOr Wind Farm Applications (SOWFA) is a high-fidelity large-eddy simulation tool that is used for wind farm studies [24] and will be used to compute the actual state, x, in this paper. SOWFA uses an actuator line or disk model to study turbines in the atmospheric boundary layer. SOWFA solves the three-dimensional unsteady spatially filtered incompressible Navier-Stokes equations and transport of potential temperature, which takes into account the thermal buoyancy and Earth rotation (Coriolis) effects in the atmosphere. Finally, SOWFA calculates the unsteady flow field and is used to compute power output at each turbine. This is a computationally expensive tool, e.g., a 10-minute two-turbine simulation can take two days to run on NREL's supercomputer using an actuator line representation of the turbine. For this research, point measurements in the SOWFA "field" are time-averaged and used with the reduced-order model to predict the instantaneous flow field. Further details can be found in [25, 26].

3.3. Kalman Filter

A Kalman filter is used to integrate the the optimal measurements of the actual state from SOWFA with the reduced-order model. A similar approach combining DMD and a Kalman filter was used in [16] and is standard practice in the controls/system literature. The Kalman filter is able to provide a computationally efficient algorithm for estimating the state based on measured outputs [27, 28]. Consider the reduced-order model of the system, defined in Section 3.1, with added noise:

$$z_{k+1} = Fz_k + w_k \tag{20}$$

$$y_k = Hz_k + v_k, \tag{21}$$

where $w_k \in \mathcal{R}^r$ is the process noise, $v_k \in \mathcal{R}^r$ is the measurement noise, $z_k \in \mathcal{R}^r$, and $y_k \in \mathcal{R}^r$ are the reduced-order states and outputs, respectively.

The standard Kalman filter can be implemented using the approach outlined in [28]. The Kalman filter uses measurements, y_k from Section 2 to update the estimate of the state at a particular time step. To implement the Kalman filter, the properties of the process noise w_k and the measurement noise v_k should be known or estimated. Typically, the covariance matrices, Q_k and R_k, of the process noise and the measurement noise, respectively, can be determined by $Q_k = E(w_k w_k^T)$ and $R_k = E(v_k v_k^T)$. This indicates that the process noise and measurement noise are independent. In the wind farm application, this information about the noise is not known. Hence, Q_k and R_k are tuned to estimate the noise. Especially for wind farm simulations, R_k is expected to be small since exact measurements can be taken from the simulations. Q_k is tuned such that all the modes of the reduced-order model are weighted equally. Another approach to defining Q_k could be to weigh the modes differently, e.g., assign different weights to different modes. The standard Kalman filter is initialized by:

$$\hat{z}_0^+ = E(z_0)$$

$$P_0^+ = E[(z_0 - \hat{z}_0^+)(z_0 - \hat{z}_0^+)^T],$$

where $\hat{z}_0^+ = U_r^T x_0$ is the initial state estimate and P_0^+ is the initial covariance on the state error. For the wind farm example, the initial covariance, P_0^+, is set to be I_r. The remainder of the Kalman filter is evaluated as

$$\begin{aligned}
\text{Covariance:} \quad & P_k^- = F P_{k-1}^+ F^T + Q_{k-1} \\
\text{Kalman Gain:} \quad & K_k = P_k^- H^T (H P_k^- H^T + R_k)^{-1} \\
\text{State Estimate:} \quad & \hat{z}_k^- = F \hat{z}_{k-1}^+ \\
\text{Measurement Update:} \quad & \hat{z}_k^+ = \hat{z}_k^- + K_k (y_k - H \hat{z}_k^-) \\
\text{Covariance Update:} \quad & P_k^+ = (I - K_k H) P_k^-
\end{aligned}$$

where the superscript "$-$" indicates the settings of the filter before the measurement update and "$+$" indicates after the measurement update. Measurements from the flow are integrated into the reduced-order model and the reduced-order state can be projected back to the full-order state using (6). This estimated state is compared with the actual state obtained using SOWFA.

4. Results

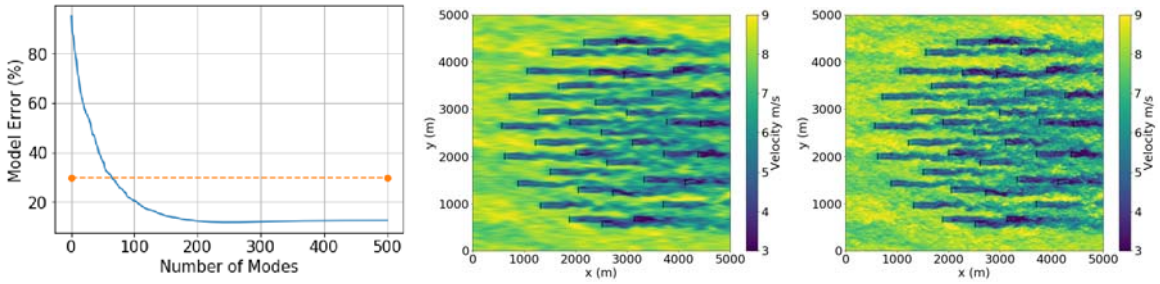

Figure 1. This figure shows the results of training the reduced-order model to the high-fidelity model, SOWFA. (Left) show the percent difference between the actual state and the estimated state. The resulting reduced-order model is shown in the middle and the results from SOWFA are shown on the right.

To demonstrate the sparse-sensor placement framework introduced in the previous sections, we use a 38-turbine wind farm, with each turbine reprsented by a vertical balck line, as shown in Figure 1 (right). The turbines are simulated as NREL 5-MW turbines [29] encountering a mean wind speed of $U_\infty = 8\,\text{m/s}$ and a turbulence intensity of approximately 6% in a neutral boundary layer. The smallest spacing between turbines is approximately 3.0 rotor diameters. The computational domain is 5 km in the x direction, 5 km in the y-direction, and 1 km in the z-direction. The grid spacing is 10 m with 500 points in the x-direction, 500 points in the y-direction, and 100 points in the z-direction. The hub-height flow field was recorded every 2 s, and the flow was sampled at 250 points in the x-direction and 250 points in the y-direction resulting in 62,500 total points. The results presented in this section were simulated using the reduced-order model and SOWFA. For this study, 38 turbines were run for 2000 s using 500 cores. The simulation took 2 days using an actuator disk representation of each turbine.

4.1. Number of Sensors

First, the reduced-order model was computed using 150 snapshots of data for DMD. The number of sensors was determined to achieve the user-specified threshold, ϵ, quantifying the difference between the actual state and the estimated state. The actual state was the SOWFA training

data and the estimated state was the output generated by the reduced-order model. Because this is a high-dimensional system, a MapReduce technique is used to obtain the singular-value decomposition of a tall-skinny matrix [30]. In this case, the user-specified threshold was set to a total difference of 30% using (17) between the actual state and the estimated state. This user threshold was arbitrarily chosen and smaller values could be chosen in the future. Choosing a higher user-specified threshold results in a fewer number of sensors needed to estimate the flow within that tolerance. The threshold chosen in this paper demonstrates the performance achieved with fewer sensors and a higher overall user-specified threshold. It is important to note that wind farm control will require the velocities at the turbines to be accurate; not the entire flow field. A significant portion of the error comes from trying to identify all the points in the flow; points not near turbines. Figure 1 (left) shows the error between the estimated and actual states decreasing as additional modes are added, i.e., as the dimension of the model is increased. This figure indicates that 64 modes are sufficient for achieving this threshold, shown by the red line. The resulting reduced-order model is shown in Figure 1 (middle). As mentioned in previous sections, the order of the model determines the number of sensors used to estimate the state. Extensions of this algorithm have shown that more sensors can be added but has not been addressed in this work [7]. Since 64 sensors is a significant number of sensors, it is likely that much fewer would be actually implemented in the field. Sensor models can be incorporated for sensors that take multiple measurements, i.e., lidar.

4.2. Sensor Locations

Next, the optimal locations of the selected number of sensors were determined using the algorithm discussed in Section 2.2, where x represents the velocities, y represents the measurements in the flow, and z is the velocities projected onto a subspace. Figure 2 (left) shows the error in the model using random vs. optimal sensor locations. This shows that this algorithm always produces a smaller error in estimating the flow over randomly placed sensors. In addition, the benefit of optimally placed sensors decreases as you add more sensors. The optimal sensor locations for two different model orders (20 and 100 sensors) are shown in Figure 2 (middle and right). There are a few important takeaways from this analysis. First, the sensor locations are clustered within downstream turbine wakes; especially downstream turbines operating in the wake of more than one turbine. Downstream turbine wakes have higher turbulence and induce higher uncertainties and may hinder the estimate of the flow field. Another observation is that many of the measurements are located near each other. One potential reasoning for these nearby measurements is to help characterize the fluctuations/turbulence in the flow to better estimate the flow field. This indicates that a single sensor may be able to measure each of those nearby points. For example, a lidar can measure multiple points at a time. In addition, a met tower could be placed nearby, and the distance between the measurement points and the met tower would indicate the reliability of those measurements. Distinct weights could be used in the Kalman filter to incorporate that additional uncertainty. Lastly, it is interesting to note that in the 20 sensor case (Figure 2 (middle)), the sensor is placed far downstream and deep within the wind farm. This part of the wind farm has an area of high uncertainty and is critical for estimating the flow field.

4.3. Model Performance

Finally, the model performance is assessed with 64 sensors in a wind farm to estimate the flow field. We compare 64 randomly placed sensors sampled from a uniform distribution and 64 optimally placed sensors calculated using the method described in Section 2. The results are shown in Figure 3. The leftmost column shows a snapshot of the actual state generated from SOWFA. This snapshot is from a test data set that has not been used to generate the reduced-order model. This data set contains 100 snapshots at 2 s time intervals. The reduced-order

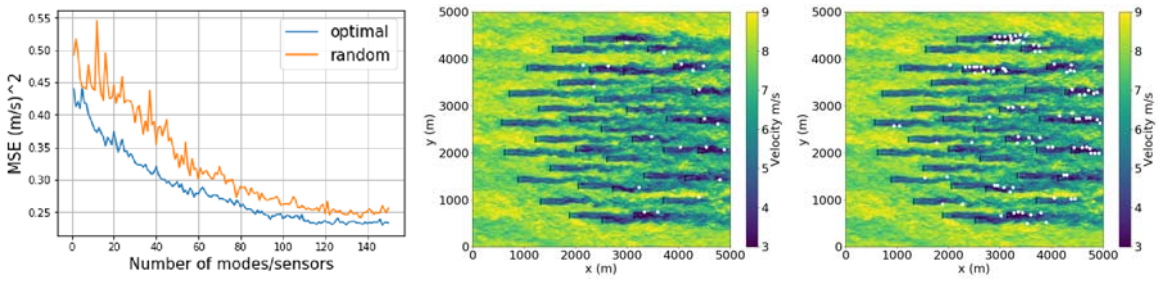

Figure 2. The left plot shows the mean square error between the actual state and the estimated state as a function of the number of modes/sensors in the system. Optimal locations for 20 sensors (middle) and 100 sensors (right). The sensor locations are indicated in white and are plotted on top of the SOWFA simulation, i.e., the actual state.

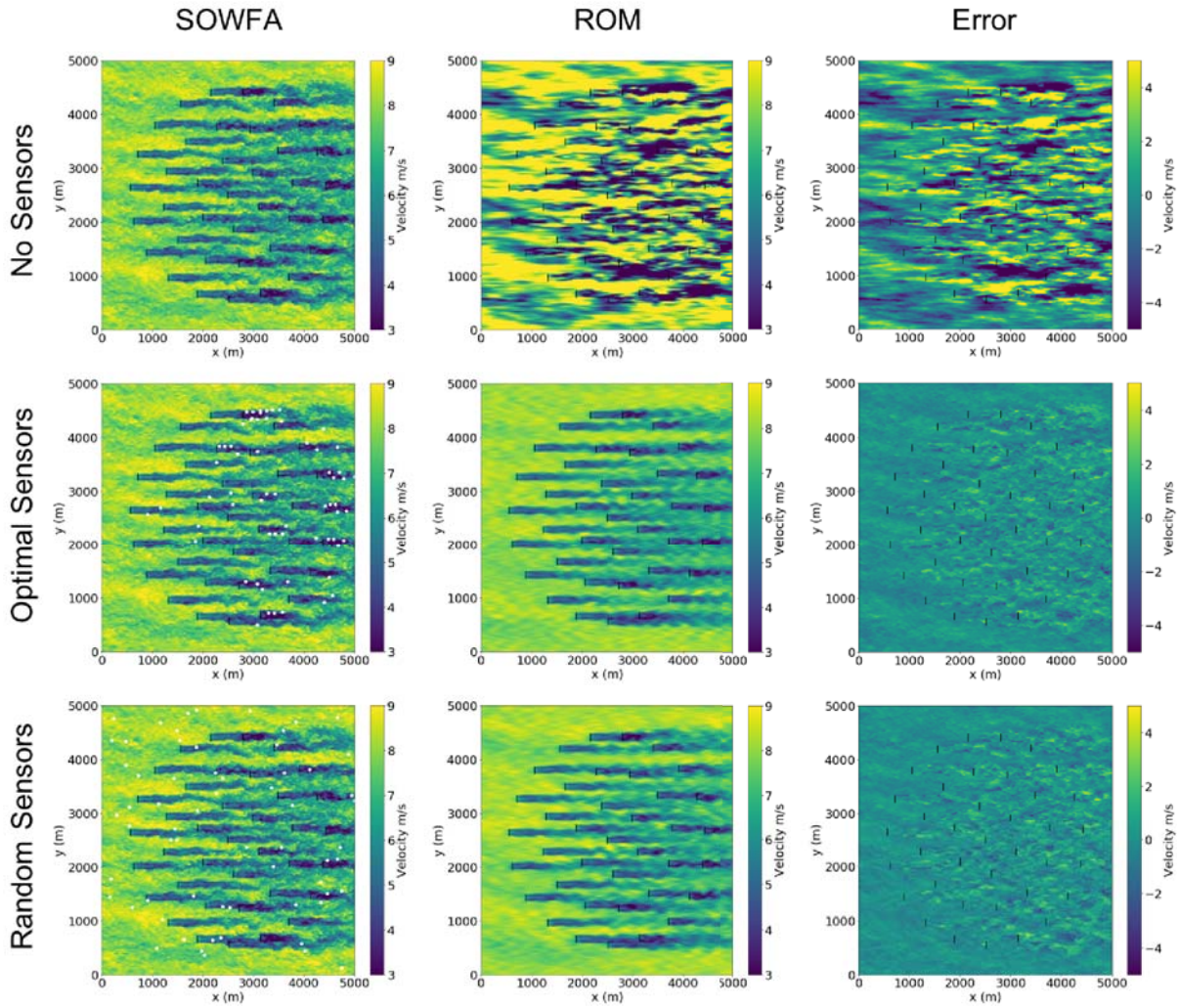

Figure 3. Analysis of SOWFA compared with the reduced-order model (ROM) at time step t = 200 s. The reduced-order model is simulated using no sensors (top row), optimal measurements using 64 senors (middle row), and random measurement locations using 64 sensors (bottom row). The errors between SOWFA and the reduced-order model are shown in the far-right column.

model was run for 100 time steps to evaluate its performance relative to SOWFA using different measurement inputs. The top plot shows the SOWFA results with no sensors. The second plot on the left shows the locations of the 64 optimally placed sensors. The third plot on the left shows the locations of 64 random sensors.

Next, the middle column shows the output of the reduced-order model with the measurements from the sensors integrated using a Kalman filter. The error between the reduced-order model and SOWFA is given on the far-right column. The results of the reduced-order model with no sensors show a poor performance in capturing the test data set. Random sensors provide additional information to the reduced-order model, and the reduced-order model performs 80% better overall in capturing the state than the no sensor case. With the optimal sensor locations, the reduced-order model does approximately 8% better in estimating the flow field in comparison with the random sensor locations.

5. Conclusions

This paper presented a sparse-sensor placement algorithm for a wind farm to optimally reconstruct the flow field within a user-specified threshold. The model order and corresponding number of sensors was determined based on this user-specified threshold of the error between the actual state and the estimated state. The optimal sensor locations were then determined using a data-driven sparse-sensor placement algorithm. It was shown that using these sensor locations leads to better a estimation of the flow field than randomly selected sensor locations.

Future work will include integrating noisy measurements from turbines. This will allow fewer additional sensors to be deployed overall. The objective function will be constructed to handle multiple or different objectives, such as estimating power throughout a wind farm using sparse sensing and performing a wind resource assessment. In addition, we will also incorporate more wind directions with a realistic wind rose, which would change the turbines that are downstream and determine their importance based on the probability within the wind rose. Finally, measurement points may be able to be aggregated and captured with one physical sensor. Physical sensor models of these various sensors, such as met towers, lidars, sodars, etc., will be introduced to account for various amounts of noise/uncertainty in different sensing devices.

6. Acknowledgments

The Alliance for Sustainable Energy, LLC (Alliance) is the manager and operator of the National Renewable Energy Laboratory (NREL). NREL is a national laboratory of the U.S. Department of Energy, Office of Energy Efficiency and Renewable Energy. This work was authored by the Alliance and supported by the U.S. Department of Energy under Contract No. DE-AC36-08GO28308. Funding was provided by the U.S. Department of Energy Office of Energy Efficiency and Renewable Energy, Wind Energy Technologies Office. The views expressed in the article do not necessarily represent the views of the U.S. Department of Energy or the U.S. government. The U.S. government retains, and the publisher, by accepting the article for publication, acknowledges that the U.S. government retains a nonexclusive, paid-up, irrevocable, worldwide license to publish or reproduce the published form of this work, or allow others to do so, for U.S. government purposes.

References

[1] S. Boersma, B. Doekemeijer, P. Gebraad, P. Fleming, J. Annoni, A. Scholbrock, J. Frederik, and J. van Wingerden, "A tutorial on control-oriented modeling and control of wind farms," in *American Control Conference*. IEEE, 2017, pp. 1–18.

[2] K. E. Johnson and N. Thomas, "Wind farm control: addressing the aerodynamic interaction among wind turbines," in *American Control Conference*. IEEE, 2009, pp. 2104–2109.

[3] C. L. Bottasso, S. Cacciola, F. Campagnolo, and J. Schreiber, "Wake detection for wind farm control–formulation and validation," in *34th Wind Energy Symposium*, 2016, p. 1741.
[4] F. Campagnolo, V. Petrović, C. L. Bottasso, and A. Croce, "Wind tunnel testing of wake control strategies," in *American Control Conference*. IEEE, 2016, pp. 513–518.
[5] B. Doekemeijer, S. Boersma, L. Pao, and J. van Wingerden, "Ensemble kalman filtering for wind field estimation in wind farms," in *American Control Conference*. IEEE, 2017, pp. 19–24.
[6] C. R. Shapiro, J. Meyers, C. Meneveau, and D. F. Gayme, "Dynamic wake modeling and state estimation for improved model-based receding horizon control of wind farms," in *American Control Conference*. IEEE, 2017, pp. 709–716.
[7] K. Manohar, B. W. Brunton, J. N. Kutz, and S. L. Brunton. (2017) Data-driven sparse sensor placement for reconstruction. [Online]. Available: https://arxiv.org/abs/1701.07569
[8] Z. Drmac and S. Gugercin, "A new selection operator for the discrete empirical interpolation method—improved a priori error bound and extensions," *SIAM Journal on Scientific Computing*, vol. 38, no. 2, pp. A631–A648, 2016.
[9] P. J. Schmid, "Dynamic mode decomposition of numerical and experimental data," *Journal of fluid mechanics*, vol. 656, pp. 5–28, 2010.
[10] P. J. Schmid, L. Li, M. Juniper, and O. Pust, "Applications of the dynamic mode decomposition," *Theoretical and Computational Fluid Dynamics*, vol. 25, no. 1-4, pp. 249–259, 2011.
[11] C. Rowley, "Model reduction for fluids, using balanced proper orthogonal decomposition," *International Journal of Bifurcation and Chaos*, vol. 15, no. 03, pp. 997–1013, 2005.
[12] S. Lall, J. E. Marsden, and S. Glavaški, "A subspace approach to balanced truncation for model reduction of nonlinear control systems," *International journal of robust and nonlinear control*, vol. 12, no. 6, pp. 519–535, 2002.
[13] M. Loève, *Probability Theory: Foundations, Random Sequences*. New York: D. Van Nostrand Company, 1955.
[14] G. Berkooz, P. Holmes, and J. L. Lumley, "The proper orthogonal decomposition in the analysis of turbulent flows," *Annual review of fluid mechanics*, vol. 25, no. 1, pp. 539–575, 1993.
[15] N. Hamilton, B. Viggiano, M. Calaf, M. Tutkun, and R. B. Cal, "A generalized framework for reduced-order modeling of a wind turbine wake," *Wind Energy*.
[16] G. Iungo, C. Santoni-Ortiz, M. Abkar, F. Porté-Agel, M. Rotea, and S. Leonardi, "Data-driven reduced order model for prediction of wind turbine wakes," in *Journal of Physics: Conference Series*, vol. 625, no. 1. IOP Publishing, 2015, p. 012009.
[17] J. Annoni and P. Seiler, "A method to construct reduced-order parameter-varying models," *International Journal of Robust and Nonlinear Control*, vol. 27, no. 4, pp. 582–597, 2017.
[18] J. Annoni, J. Nichols, and P. Seiler, "Wind farm modeling and control using dynamic mode decomposition," in *34th Wind Energy Symposium*, 2016, p. 2201.
[19] J. L. Proctor, S. L. Brunton, and J. N. Kutz, "Dynamic mode decomposition with control," *arXiv preprint arXiv:1409.6358*, 2014.
[20] T. Burton, D. Sharpe, N. Jenkins, and E. Bossanyi, *Wind energy handbook*. John Wiley & Sons, 2001.
[21] L. Y. Pao and K. E. Johnson, "Control of wind turbines," *Control Systems, IEEE*, vol. 31, no. 2, pp. 44–62, 2011.
[22] M. Budisic, R. M. Mohr, and I. Mezic, "Applied Koopmanism," *arXiv:1206.3164*, 2012.
[23] I. Mezic, "Analysis of fluid flows via spectral properties of the Koopman operator," *Annual Review of Fluid Mechanics*, vol. 45, pp. 357–378, 2013.
[24] M. J. Churchfield, S. Lee, and P. Fleming, "Simulator for wind farm applications," National Renewable Energy Laboratory (NREL), Golden, CO (United States), Tech. Rep., 2012.
[25] M. J. Churchfield, S. Lee, P. J. Moriarty, L. A. Martinez, S. Leonardi, G. Vijayakumar, and J. G. Brasseur, "A large-eddy simulation of wind-plant aerodynamics," *AIAA paper*, vol. 537, p. 2012, 2012.
[26] M. J. Churchfield, S. Lee, J. Michalakes, and P. J. Moriarty, "A numerical study of the effects of atmospheric and wake turbulence on wind turbine dynamics," *Journal of turbulence*, no. 13, p. N14, 2012.
[27] R. E. Kalman, "A new approach to linear filtering and prediction problems," *Journal of Basic Engineering*, vol. 82, no. 1, pp. 35–45, 1960.
[28] D. Simon, *Optimal state estimation: Kalman, H infinity, and nonlinear approaches*. John Wiley & Sons, 2006.
[29] J. Jonkman, S. Butterfield, W. Musial, and G. Scott, "Definition of a 5-MW reference wind turbine for offshore system development," *National Renewable Energy Laboratory, Golden, CO, Technical Report No. NREL/TP-500-38060*, 2009.
[30] J. Dean and S. Ghemawat, "Mapreduce: simplified data processing on large clusters," *Communications of the ACM*, vol. 51, no. 1, pp. 107–113, 2008.